

Injection Type Effects on Pulverized Biomass (solid olive waste) Combustion in a 50 kW Combustor

Abdallah Elorf^{*}, Brahim Sarh^{*}, Sylvie Bonnamy^{**}, Mohamed Asbik^{***}, Yassine Rahib^{****}, Jamal Chaoufi^{****}

^{*} ICARE CNRS, 1C, Avenue de la Recherche Scientifique, 45071 Orléans Cedex 2, France

^{**} ICMN-CNRS, UMR7374, Université d'Orléans, Orléans, France

^{***} ERTE, Ecole Normale Supérieure d'Enseignement Technique, UM5, BP 6207 Avenue des FAR Rabat 10100, Maroc

^{****} LETSMP Ibn Zohr University, Faculty of sciences – B.P 8106, Agadir, Maroc

*Corresponding author: Abdallah ELORF

Tel.: +33751375062

E-mail address: elorf.abdel@gmail.com

Received: 29.01.2019 Accepted: 22.03.2019

Abstract- The paper describes a 3D numerical simulation of pulverized solid olive waste (OW) combustion in a vertical combustor. This study is developed, in order to design a new efficient burner which operates with olive waste as a biomass fuel. Two types of injection modes are studied. The first named (R) where the biomass particles is perpendicularly injected to symmetric axis close to the co-flow entry by four injection square shape tubes and the second named (P) where particles are injected in parallel to the furnace central axis. The mean diameter of the pulverized particles is about 70 μm . The designed system is a vertical cylindrical furnace with swirling co-flow burner entry. The k- ϵ , mixture fraction PDF and discrete phase DPM models are used for turbulence closure, turbulence-chemistry interactions and tracking the particle motion respectively. Results show that the flame is more stabilized in the recirculation zones and achieved the higher temperature at 1560 K for (R) case. The particles residence time inside to the combustor is very important for the (R) case in comparison to (P) case. The analyses and comparison of the formed species for CO, CO₂ and NO_x formation profiles at several longitudinal locations between (R) and (P) cases are performed.

Keywords: Pulverized biomass, Olive waste Combustion, CFD, Swirling flame, Numerical simulation.

1. Introduction

The biomass can be considered as a very momentous fuel for heating and electricity production, following his contribution to reduce greenhouse gas emissions. Combustion is one of famous methods of biomass energy recovery. It's noted that the areas of application of biomass combustion are numerous and interesting, such as pilot-scale and large-scale boilers, furnace and stoves [1-2]. In addition, to meeting society's energy needs the biomass combustion in mixing with another fossil fuel, contribute to reducing polluting emissions. Moreover, the conversion biomass technologies know a great development and elevate new opportunities for growth and economic recovery. [3-4].

Solid olive waste (OW) is a byproduct of the process of extracting the olive oil made skins, residue of the pulp and fragments of the cores. About 1.5 million tons of olives are produced every year and 675,000 tons of olive wastes are results [5] in Morocco. We are facing two major problems: the first is environmental problems linked to management of this waste; the second is linked to the energy requirements. Effective use of OC in energy recovery will be a good solution to solve these problems. the importance of the higher olive waste high heating value (HHV) allow to energy recovery and compare his energetic efficiency to that of soft coal and wood mostly in the regions where the olive tree are high. [6-7].

Lockwood et al. (1980) and Bermudez et al. (1997) [8-9] have developed several code of computational fluid dynamic

(CFD) to solving equations generated during pulverized coal combustion. Eaton et al. 1999 [10] studied the CFD modelling methodology as applied to combustion processes. Different combustion models have been presented. The categories of necessary data for validation of the detailed combustion codes forecasts are considered. A comparison between results of simulations and experimental data was made.

The coal combustion modelling limitation due to simplified models used to simulate the various coal conversion phases (devolatilization and char combustion) has studied by Korytnyi et al. [11] and Williams et al. [12]. Two separately models were developed by Yin et al. [13-14-15] using the integrated model of commercial software Fluent. First 3D model developed from entry boundary conditions of the experience and second is a one-dimensional model of the transport equations for fixed-bed modelling. Scharler et al. [16-17] studied the numerical simulation of biomass combustion in an industrial furnace (0.55 MW). This research group used the Finite Rate Chemistry model to simulate the wood flame.

In 2013 Elfasakhany et al. [18] investigated the experimental and numerical studies on pulverized wood flame in a pilot-scale combustor. The objectives of this work were to study the basic structures of the pulverized wood flame, to identify the main reasons that caused emissions of volatile substances and unburnt.

Ma [19] modeled coal and biomass combustion and proves that it's possible to predict the flame behavior. Arafat et al [20] studied radiative and convective performance effects in pulverized Russian coal flame. Recently in (2015) Stroh et al. [21] performed a 3D digital simulation with CFD code ANSYS FLUENT 14, to investigate the combustion characteristics of pulverized solid fuel.

Obaidullah et al. [22] studied particle emissions from Small scale biomass combustion biomass combustion. Mayin et al. [23-24] studied numerically Bag-type collector flow field in biomass energy of power plant and combustion of circulation fluidized bed biomass boiler. Wickramasinghe et al. [25] Developed a numerical model to analyze the transport phenomena of suspension biomass combustor with two chambers. The CFD model was based on Eulerian-Lagrangian concept, which tracks each biomass particle individually with association of multiple physics and thermo-chemical properties.

To the best knowledge of the authors, the first olive waste (OW) combustion work was study carried out on the possibility of using OW as source of energy in 1998 was done by Alkhamis et al [26]. One year ago Khraisha et al [27] studied the direct OW combustion in fluidized bed combustor. In 2007 Varol et al [28] studied the OW combustion characteristics with different air inlet conditions.

The aim of this work is to investigate a 3D modelling of pulverized OW combustion in vertical pilot-scale combustor with different type of biomass injection. Two cases (R) and (P) with parallel and perpendicular OW particles injection to the combustor symmetrical axis are studied. The Discrete Phase Model (DPM) to study OW particles motion is used.

Flow turbulence was modeled using k-ε model. To predict the interaction between turbulence and chemistry the PDF model is used. The obtained results regarding flow, axial velocity contours, temperature profiles, CO and CO₂ concentrations and NO_x formation profiles are presented for (R) and (P) cases.

1. Presentation of the Global Process

The olive waste particles can be used to generate the electric power as the conventional solid fuel (coal). As shown in Figure 1, combustion generates high temperature steam and high pressures; Turbine is drive by steam and alternator by turbine in order to produce the electricity. The residual heat from the turbine can be used to heat building or other facilities.

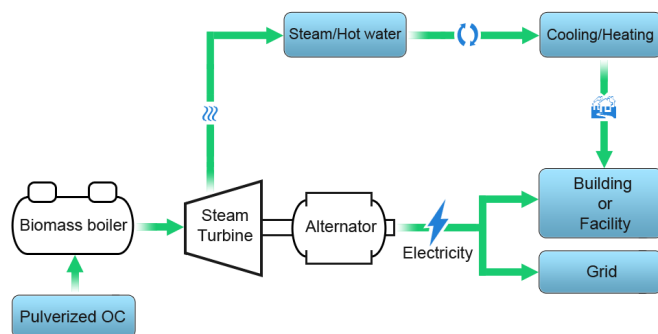


Fig. 1. Process of combined heat and co-generation

2. Combustor and the Operating Condition

Schematic figure of the combustor is illustrated in Figure 2. The atmospheric pressure combustors include burner with co-flow jet, four perpendicular particle injection tubes and a combustion chamber. A swirling motion is given to the air in the central entry (swirl flow entry). The burner is a cylindrical tube with co-axial air inlet diameter $d = 80$ mm, length of $2.25 d$ and inner air inlet diameter of $0.75 d$. The particles injectors are four square tubes with a length of $1.25 d$. The olive cake particles are injected throughout tubes with air. The length of the cylindrical combustor is $18.75 d$ and diameter is $6.25 d$.

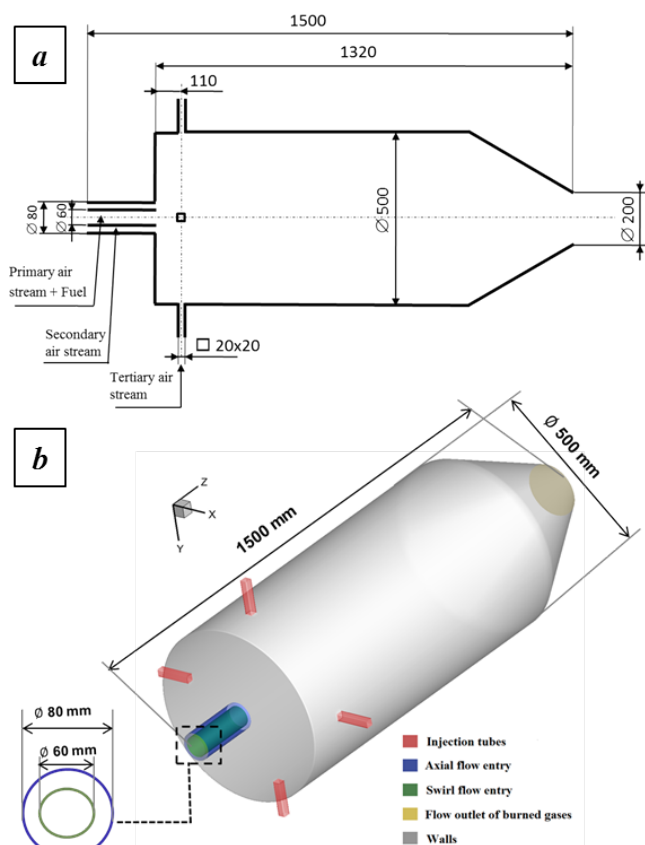


Fig. 2. Schematic figure of the combustor: (a) 2D view; (b) 3D view

The inlet air temperature is $T_0=300\text{ K}$ and the swirl number used for swirl flow entry is $S_n=1.2$. The air mass flow rate of swirl and axial flows entry are $\dot{m}_{swirl} = 4.55\text{ g/s}$ and $\dot{m}_{air} = 2.83\text{ g/s}$ respectively. The particles biomass mass flow rate is $\dot{m}_{OW} = 0.561\text{ g/s}$.

The HHV of biomass used in this is 20.2 MJ/kg measured using a bomb calorimetric available in the laboratory. The ultimate and approximate analyses used of olive cake are presented in Table 1 [29].

Table 1. Olive waste composition (wt. %)

Proximate Analysis (%)		Ultimate analysis (%)	
Volatile Matter (VM)	64	Carbon (C)	59
Fixed Carbon (FC)	23.2	Hydrogen (H)	8.5
Ash (Ash)	6.5	Nitrogen (N)	1.5
Moisture (M)	6.3	Oxygen (O)	31

3. Computational Method and Modeling

3.1. Grid generation

A quarter of the total configuration is chosen to cover the computational domain. To create mesh we have used a technique of multi block. 29 blocks have been created, 28

blocks with hexahedral mesh and the 29th with mixing of hexahedral and prism mesh. The mesh is plotted for the total domain (Figure 3a) and for the computational domain (Figure 3b). The CFD simulations were conducted with a grid spacing of 1956384 cells in computational domain (Figure 3-b).

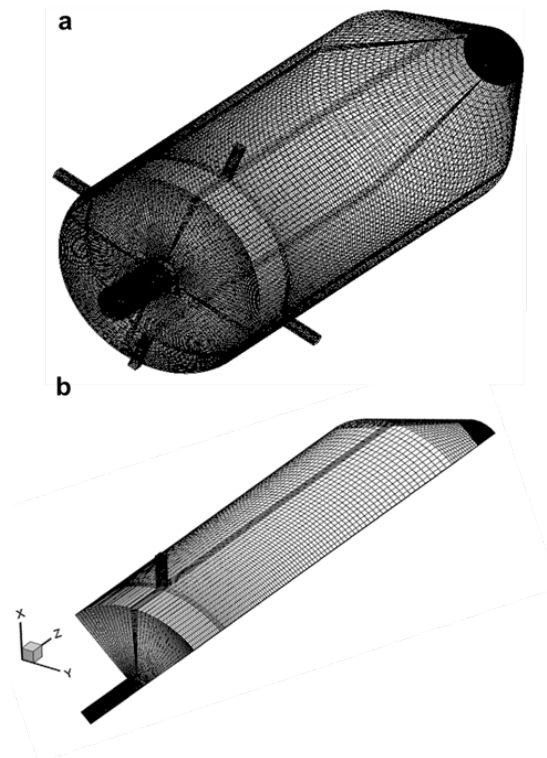


Fig. 3. Computational grid for the mesh: a) All domain b) Computational domain

3.2. Numerical method

The finite volume method using the commercial software ANSYS14 is used to solve all equations systems. P1 model was chosen for radiation model. Flow turbulence was modelled by k-ε model. Non-premixed combustion model was chosen with the mixture fraction PDF for interaction between chemistry and turbulence. Solid phase was modelled using Lagrangian method by discrete phase model (DPM).

3.3. Flow modeling

As mentioned in the introduction, the k-ε model is used, where k and ε are calculated using the two following transportation equations:

$$\frac{\partial}{\partial t} (\rho k) + \frac{\partial}{\partial x_i} (\rho k u_i) = \frac{\partial}{\partial x_j} \left[\left(\mu + \frac{\mu_t}{\sigma_k} \right) \frac{\partial k}{\partial x_j} \right] + G_k + G_b - \rho \varepsilon \quad (1)$$

$$\frac{\partial}{\partial t} (\rho \varepsilon) + \frac{\partial}{\partial x_i} (\rho \varepsilon u_i) = \frac{\partial}{\partial x_j} \left[\left(\mu + \frac{\mu_t}{\sigma_\varepsilon} \right) \frac{\partial \varepsilon}{\partial x_j} \right] + C_{1\varepsilon} \frac{\varepsilon}{k} G_k - C_{2\varepsilon} \rho \frac{\varepsilon^2}{k} \quad (2)$$

Where the turbulent viscosity μ_t is given by the relationship of Prandtl-Kolmogorov as

$$\mu_t = \rho C_\mu \frac{k^2}{\varepsilon} \quad (3)$$

In the above equation, $G_k = \mu_t \left(\frac{\partial U_j}{\partial x_i} + \frac{\partial U_i}{\partial x_j} \right) \frac{\partial U_i}{\partial x_j}$ and $G_b = \beta g_i \frac{\mu_t}{Pr_t} \frac{\partial T}{\partial x_i}$ represents the turbulence kinetic energy generation due respectively to the mean velocity gradients and buoyancy.

$C_{1\varepsilon}$ and $C_{2\varepsilon}$ are constants and $\sigma_k, \sigma_\varepsilon$ are turbulent Prandtl numbers for k and ε respectively, more details are given in reference [30-31]. The constants $C_{1\varepsilon}, C_{2\varepsilon}, \sigma_k$ and σ_ε are given by the Launder and Sharma model as mentioned below:

Table 2: The k- ε model constants

C_u	$C_{1\varepsilon}$	$C_{2\varepsilon}$	σ_k	σ_ε
0.09	1.44	1.92	1.0	1.3

3.4. Model of Radiation P-1:

The P-1 equation is interested in the incident radiation distribution (G) in a computation domain as show in equation below:

$$\nabla(\Gamma \nabla G) - \alpha G + 4\alpha \sigma T^4 = 0 \quad (4)$$

Here, α is the absorption coefficient, σ is constant and $\Gamma \left(= \frac{1}{3(\alpha + \sigma_s) - C\sigma_s} \right)$ is the radiative flux vector with σ_s is the scattering coefficient and C the linear-anisotropic phase function.

More details about P-1 radiation model in reference [32].

3.5. Mixture fraction model

The principle of the approach for modeling a non-premixed flame consists in linking the thermochemical quantities (temperature, density and mass fraction) to a scalar quantity. The model named mixture fraction PDF model.

Turbulence-chemistry interaction is modelled using a probability density function (PDF). This method is based on simplifying hypotheses; the value of mixture fraction f is giving by the solution equation below [33]:

$$\frac{\partial}{\partial x_i} (\rho u_i f) = \frac{\partial}{\partial x_i} \left(\frac{\mu_t}{\sigma_t} \frac{\partial \bar{f}}{\partial x_i} \right) + S_M \quad (7)$$

The mixture fraction variance, f'^2 is given by equation (8):

$$\frac{\partial}{\partial x_i} (\rho u_i \overline{f'^2}) = \frac{\partial}{\partial x_i} \left(\frac{\mu_t}{\sigma_t} \frac{\partial \overline{f'^2}}{\partial x_i} \right) + C_g \mu_t \left(\frac{\partial \bar{f}}{\partial x_i} \right)^2 - C_d \rho \frac{\varepsilon}{k} \overline{f'^2} \quad (8)$$

Where the values of σ_t, C_g and C_d in Eq. (8) are given by Jones and Whitelaw [33].

3.6. Discrete phase model (DPM)

The Discrete Phase Model is used to modelling the olive waste particles motion. The particles trajectory has been interpreted by integrating the force balances in particles motion equation [34].

Method of Rosin-Rammler distribution is used for particles diameter injection. The particles are considered as spherical with mean diameter of $D_{\text{mean}} = 70 \mu\text{m}$.

Equation (9) show the force balance expression acting on the particle

$$\frac{\partial \vec{u}_p}{\partial t} = F_D(\vec{u} + \vec{u}_p) + \vec{g}(\rho_p - \rho)/\rho_p \quad (9)$$

Where $F_D(\vec{u} + \vec{u}_p)$ represent the drag force; u : velocity of the fluid; u_p velocity of the particle; ρ : density of fluid and ρ_p : density of particle.

3.7. Devolatilization submodel

The one-step model is used in this work. In this model the devolatilization process is interpreted by a single Arrhenius first order reaction in the following form [35-36]:



Where V is volatiles fraction and k can be expressed by law Arrhenius as

$$k = A e^{(-E_a/RT)} \quad (10)$$

A and E are giving by Oevermann et al. [35] and respectively are $1.43 \cdot 10^4 \text{ s}^{-1}$ and 88.6 kJ/mol ,

4. Results and Discussion

4.1. Flow topology

Figure 4 present the flow topology along the furnace using streamline patterns. The flow is complex and distinct two main regions which are: the recirculation zones and the axial jet region. The first takes its shape from the neighbouring walls and it serves as an aerodynamic flame holder. The second, it locates in the centre of the furnace, and it comes as a result of the high axial velocity gradient in this region. In addition, the flow contains various critical points in its topology. Those points are positions in the flow field domain where the velocity vanishes. For the present case there are four critical points: recirculation points (red dots), the horseshoes (blue dots), separation points (repelling nodes "purple cross mark") and stagnation points (green plus mark). The recirculation points, named also the centres because they are the centres of the recirculation regions. The horseshoes appear as a pair of counter rotation vortices. They are generated as a result of the interaction between the incoming swirling flow and the perpendicular flow of the injected particles. Those vortices are small and strong, they contain a high turbulent energy and high negative velocity (see Figure 5). The separation points are characterized by the

outflow behaviour from one point to all directions, where the stream lines do not touch each other. The stagnation points (named also saddle points) are formed to the interaction between the horseshoes vortices and the recirculation vortices, on the one hand, and between the horseshoes vortices and the repelling nodes, on the other hand.

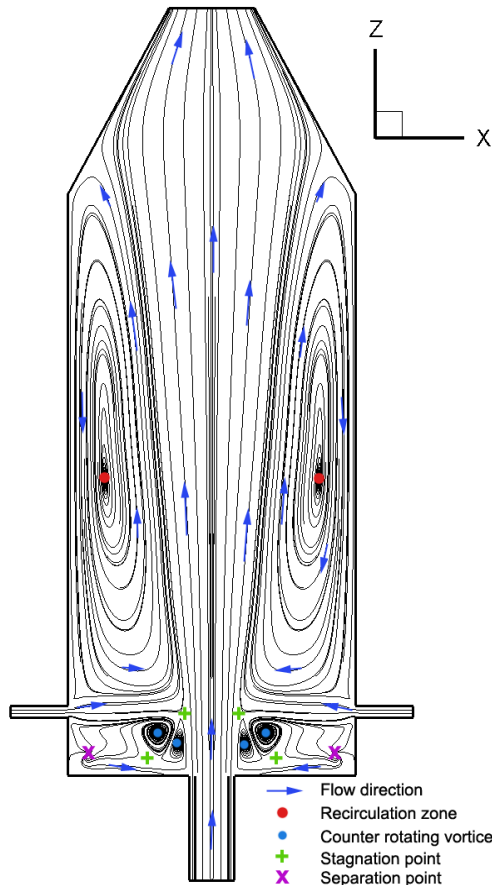


Fig. 4. Streamline patterns of the flow topology

4.2. Axial velocity and turbulence kinetic energy profiles

Figure 5 illustrates the axial velocity (a) and turbulence kinetic energy (b) contours along the combustor. High velocity gradients are identified in three regions which are: the inlet tube, the center region and at the outlet. The first high velocity gradient is due to the small confined section of the tube; the second is due to the high axial jet in the center of the burner and the third is due to the converging section at the outlet which accelerates the gas flue. Regarding the turbulence kinetic energy (Figure 5.b), there are two main regions contain high turbulent energy values. The first region is the shear layer below zones of recirculation and right of center axial jet. This region contains a high shear force which leads to high production of kinetic energy. The second region is the outlet of the furnace with converging shape, which accelerates the flow and induces a high kinetic energy.

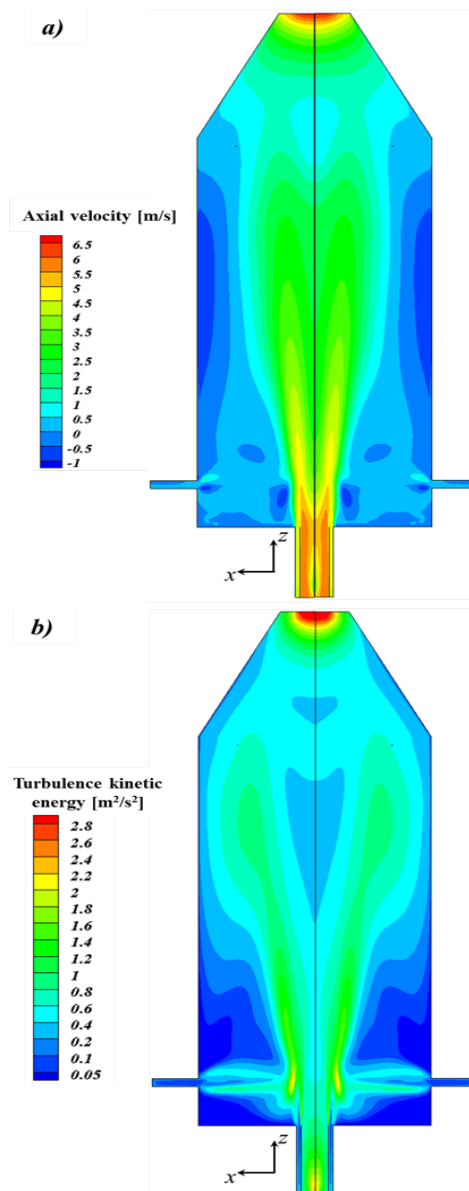


Fig. 5. Predicted axial velocity contours (a) and turbulence kinetic energy (b).

4.3. Gas temperature

Figure 6 shows the predicted temperature profile along the furnace. There is no flame in the centre region of the chamber, because of the high velocity of axial air which occurs in this region. The flame locates where the high gradient of temperature occurs, close to the particles injector outlet and in the recirculation zones. Those zones are partially filled with combustion gases and are involved in the flame stabilization when the burnt and fresh gases are in contact and the flame ignition stay permanent. The flame maximum temperature of OW (olive waste) is about 1560 K found in the centre of the flame.

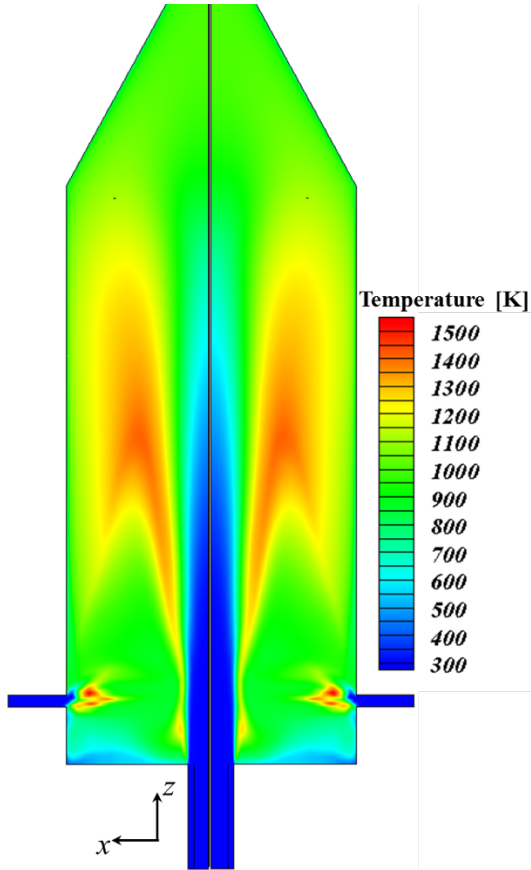


Fig. 6. Temperature distribution along the burner

4.4. Temperature and O₂ concentration profiles

Figure 7 shows the oxygen mass fraction and the flame temperature in several locations along to the combustor. The temperature and oxygen values are plotted in relative to the reference values ($T_{ref}=1560K$, $O_{ref}=0.233$) corresponding to the maximum values in the furnace. The evolution of adimensional temperature and O₂ profiles for five locations are presented. It is shown that for all the location along the furnace the low O₂ concentration zones correspond to the high gas temperature zones.

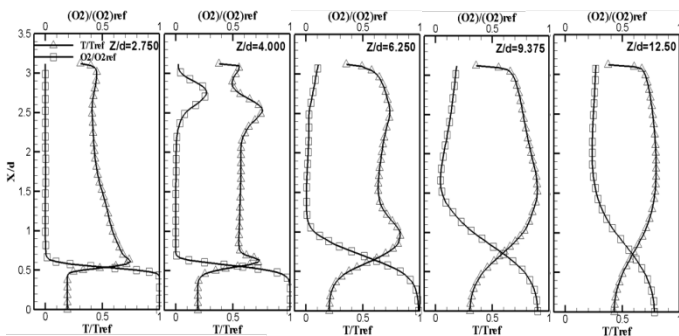


Fig. 7. Adimensional temperature and oxygen mass fraction ($T_{ref}=1560K$, $O_{ref}=0.233$)

4.5. Particles trajectory

Trajectories of four tracks OW particles entering the furnace colourful by temperature and residence time are shown in Figure 8 (a) and 8 (b) respectively. In figure 8 (a) we can see the particles temperature during devolatilization in the bottom part of the combustor and char combustion in

upper part of the combustor. According to approximate analysis presented before, olive waste contains 29.7% of char (fixed carbon + ash). The particle achieves the char combustion phase with a maximum temperature of 1600 K, and the mass continued to decrease until they leave the exit of combustor. Figure 8 (b) shows that the maximum olive waste particles residence time is about 29 s.

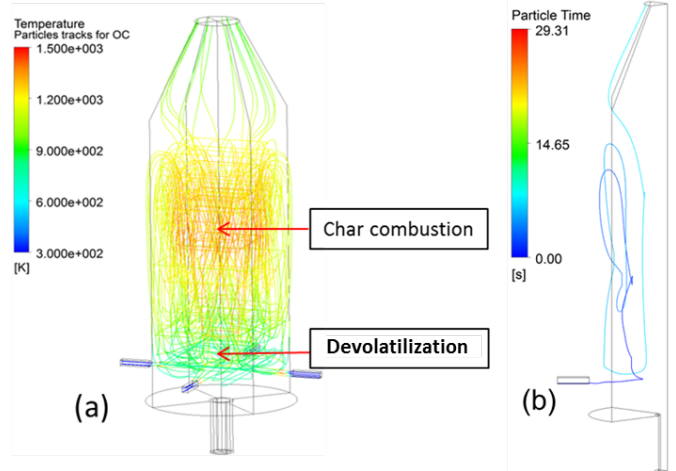


Fig. 8. Trajectory of particles colored by: (a) temperature (four tracks) and (b) residence time (one track).

4.6. Combustion products

Figure 9 shows CO₂ and CO mass fraction radials profiles in five locations along to the combustor. For all locations, we can see that the CO and CO₂ concentrations increase with the same trend until distance of $X/d = 0.4$. Then, CO mass fraction decreases until the minimum value of 0 and CO₂ increases until his higher value $(CO_2)_{ref} = 0.253$ and remains constant up to the walls.

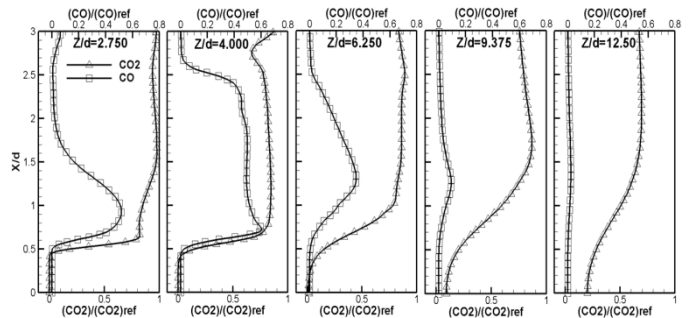


Fig. 9. Adimensional CO₂ and CO mass fractions radials profiles ($d=80$ mm, $CO_{2ref}=0.253$, $CO_{ref}=0.149$)

Figure 10 illustrates the distribution of adimensional NO_x concentration profiles in five distances along to the combustor Z/d. NO_x can be formed by nitrogen oxidation or by high speed front flame level reactions [36]. Although a maximum of NO_x mass fraction is noticed respectively at the level of the wall and at the combustor outlet. NO_x mass fraction reaches a maximum value $NO_{xref}=3.5 \times 10^{-4}$ at the combustion temperature peak at the level of recirculation zone. These values are shown in both distances along to the combustor $Z/d=4.375$ and $Z/d=5.625$ as shown in Figure 10.

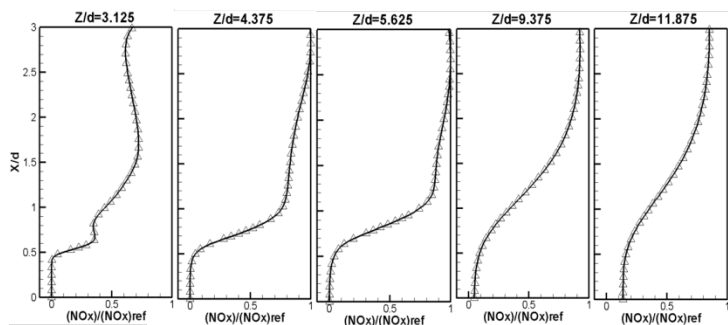


Fig. 10. Adimensional NO_x radials profiles ($d=80$ mm and $\text{NO}_{x\text{ref}}=3.5 \times 10^{-4}$)

5. Injection types effects on pulverized biomass flame

To study the effects of injections nature on flame behaviour of pulverized olive waste combustion, we have compared two cases with different injection nature. The first named (R) case: correspond to the cases studied in the section before where the particles are injected perpendicularly to the central axis, the second named (P) case: where the particles are injected in parallel to central axis with swirl air injection.

Figure 11-a present the comparison of flame temperature for the two cases. For perpendicular injection of the particles case (R) there is no flame in the center region of the chamber. The flame is located beside to the wall unlike (P) cases the flame is located in the center region of the combustor, because of high velocity of the axial air jet which occurs in this region. The comparison between the adimensional temperatures in the central axis for the two cases is given in figure 11-b. The results are divided by the reference value ($T_{\text{ref}}=1560$ K) which corresponds to the higher temperature reached for the two cases. The centerline temperature of the parallel injected particles case (P) is higher than the centerline temperature of the perpendicular injection case (R). At the combustor exit, the temperature values are close to each other of both cases.

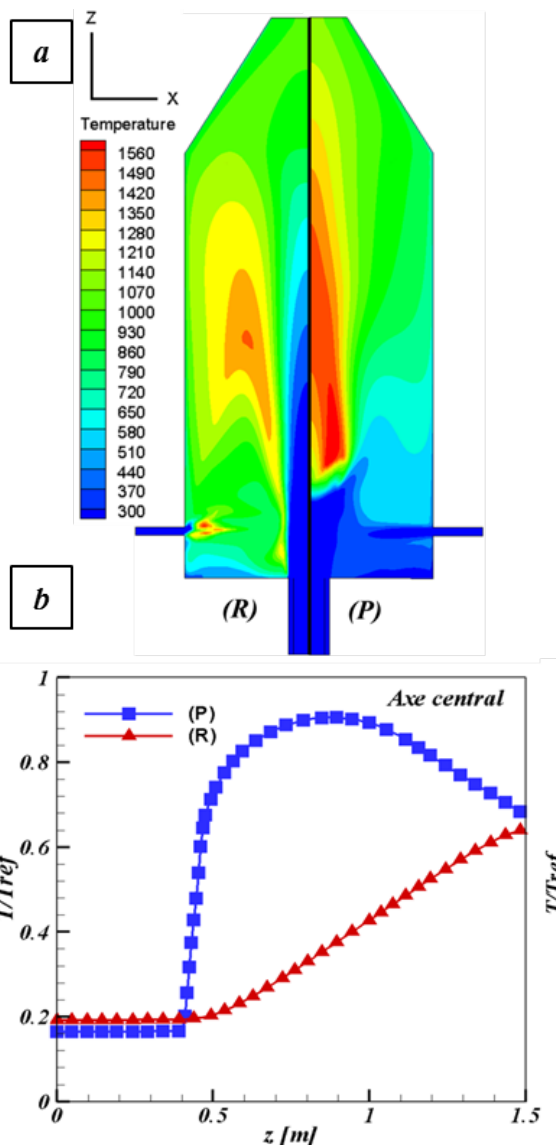


Fig. 11. a) Temperature contours, b) central axis temperature.

Figure 12 presents the adimensional profiles of CO_2 concentration in four different locations ($Z/d=5.625$, $Z/d=9.375$, $Z/d=12.50$ and $Z/d=18.75$) along to the combustor. The reference value $(\text{CO}_2)_{\text{ref}}=0.253$ is use to normalize CO_2 mass fraction, this value is related to the maximum value reached for two cases. The maximum CO_2 mass fraction value locates close to the wall condition for (R) cases and beside to central axis for (P) cases. The CO_2 mass fraction decrease for case (R) and increase for case (P) when it is far of the central axis ($r=0$ m). It is shown that the case (R) provide less CO_2 concentration in comparison with case (P) in the combustor exit ($Z/d=18.75$). Furthermore the perpendicular injection of particles helps to reduce the spread of CO_2 emissions in the furnace outlet.

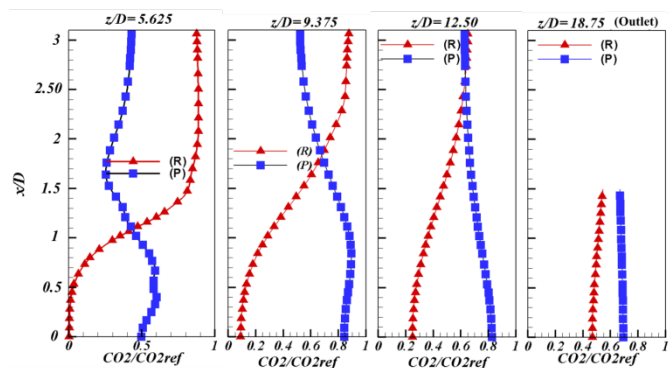


Fig. 12. Adimensional CO₂ mass fraction radial profiles for the two cases

Figure 13 shows the adimensional NO_x concentration in four longitudinal locations ($Z/d=5.625$, $Z/d=9.375$, $Z/d=12.50$ and $Z/d=18.75$ (outlet)) along to the combustor. The mass fraction of NO_x is higher respectively at the level of the wall for case (R) and close to central axis for case (P). NO_x mass fraction reaches a maximum value $NO_{xref}=3.5 \times 10^{-4}$ at the combustion temperature peak for two cases. It is shown that the case (R) dilute NO_x concentration in comparison with case (P). This propriety observed in furnace exit ($Z/d=18.75$) that the NO_x concentration is very less for case (R) than case (P).

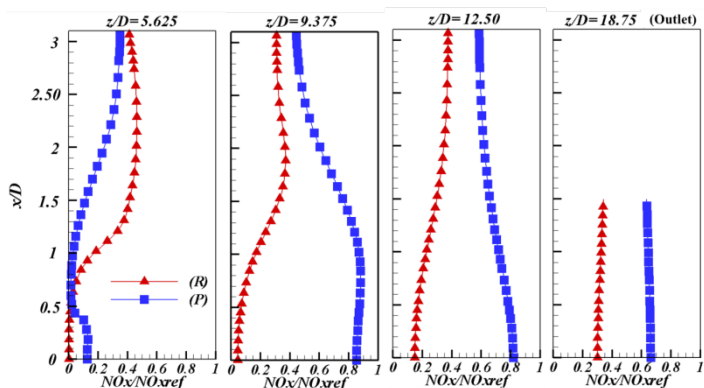


Fig. 13. NO_x mass fraction radial profiles for the two cases

Trajectories of four tracks olive waste particles entering the furnace colourful by temperature for two cases are shown in Figure 14. As shown in the figure there are no particles in the bed of combustor. There are two particles phases for all cases: devolatilization and char combustion. The char combustion corresponds to higher particles temperature for the two cases. The trajectory of the olive waste particles for case (R) is very long compared to trajectory for case (P) and consequently particle residence time is long for (R) case compared to (P) case. This is due to the flow topologies nature created in the furnace for these cases. Furthermore the perpendicular particles injection type helps to increase the time of particle stays inside to the combustor.

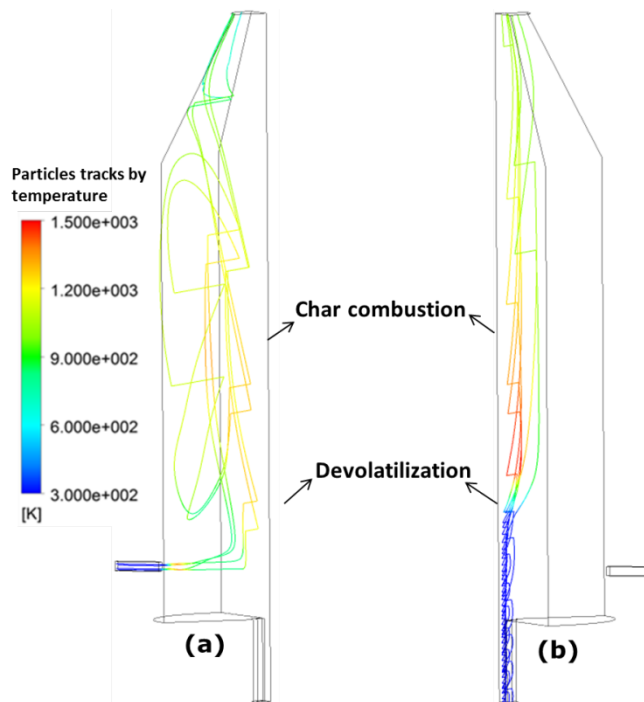


Figure 14. Trajectory of particles colored by temperature (four tracks) for two cases.

6. Conclusion

This paper summarized a 3D numerical simulation of pulverized olive waste combustion in pilot scale combustor (50kW) with different type of biomass injection. Two cases named (R) and (P) are studied. Flow turbulence was modeled using k-ε model. The Discrete Phase Model (DPM) to study OW particles motion is used. Interaction between turbulence and chemistry is predicted using PDF model. The maximum reached temperature for both cases is about 1560 K. Regarding combustion products, it is shown that the case (R) provide less CO₂ concentration in comparison with case (P). It is also shown that the case (R) dilute NO_x concentration in comparison with case (P). Concerning particles residence time, the time stays of (R) case particles is very important than (P) cases time stays inside to the combustor. However perpendicular particles injection type helps to increase the time of particle stays inside to the combustor. The results will be used to derive data for designing and optimizing the operation of a medium and large-scales combustor of pulverized biomass unit.

ACKNOWLEDGEMENTS

The Region Centre Val de Loire, France is appreciated for the funding support via theVERA-P2 project n° 2015-00099702.

References

- [1] J. Collazo, J. Porteiro "Numerical modeling of the combustion of densified wood under fixed-bed conditions", Fuel, Vol. 93, pp. 149-159, March 2012.
- [2] K.A. Al-attab, Z.A. Zainal, "Design and performance of a pressurized cyclone combustor (PCC) for high and low heating value gas combustion" Applied Energy, Vol. 88, pp. 1084-1095, 2011

- [3] Y. Chung L. A. Rosendahl, K. K. Søren, "Grate-firing of biomass for heat and power production" *Progress in Energy and Combustion Science*, Vol. 34, pp. 725-754, 2008
- [4] Xinhui Zhang, Mohsen Ghamari, Albert Ratner. "Numerical modeling of co-firing a light density biomass, oat (*Avena sativa*) hulls, and chunk coal in fluidized bed boiler" *Biomass and bio Energy*, Vol. 56, pp. 239-246, 2013.
- [5] M. Jianchun; Pengfei, Li. B. D. Bassam, A. C. Richard. "Importance of Initial Momentum Rate and Air-Fuel Premixing on Moderate or Intense Low Oxygen Dilution (MILD) Combustion in a Recuperative Furnace" *Energy& Fuels*, Vol. 23, pp. 5349-5356, 2009
- [6] H. Topala, A. T. Atimtayb, A. Durmaz "Olive cake combustion in a circulating fluidized bed" *Fuel*, Vol. 82, pp. 1049-1056, 2003
- [7] Aysel T. Atimtaya, Hu'seyin Topal "Co-combustion of olive cake with lignite coal in a circulating fluidized bed" *Fuel*, Vol. 83, pp. 859-867, 2004
- [8] F.C. Lockwood, A.P. Salooja, S.A. Syed, A prediction method for coal-fired furnaces. *Combust. Flame*, Vol. 38, 1980.
- [9] A. Bermudez, J.L. Ferrin, "Modelling and numerical solution of a pulverized coal furnace," *Proceedings of the 4th International Conference on Technologies and Combustion for Clean Environment*, Lisbon, Portugal, pp. 1-9 paper 33.1, 1997
- [10] A.M. Eaton, L.D. Smoot, S.C. Hill, C.N. Eatough, "Components, formulations, solutions, evaluation, and application of comprehensive combustion models" *Prog. Energy Combust. Sci*, Vol. 25, 4, pp. 387-436, 1999
- [11] E. Korytnyi, R. Saveliev, M. Perelman, B. Chudnovsky, E. Bar-Ziv, "Computational fluid dynamic simulations of coal-fired utility boilers: An engineering tool", *Fuel*, Vol. 88, pp.9-18, 2009.
- [12] A. Williams, R. Backreedy, R. Habib, J.M. Jones, M. Pourkashanian, "Modelling coal combustion: the current position" *Fuel*, Vol. 81-5, 605-618, 2002.
- [13] C. Yin, L. Rosendahl, S. K. Kær and H. Sørensen. "Modeling the motion of cylindrical particles in a nonuniform flow" *Chemical Engineering Science*, Vol. 58, pp. 3489-3498, 2003
- [14] Yin C., Rosendahl L., and Condra T. J. Further study of the gas temperature deviation in large-scale tangentially coal-fired boiler. *Fuel*, 82- 9, pp. 1127-1137, 2003
- [15] C. Yin, L. Rosendahl, S.K. Kær, T.J. Condra, "Use of numerical modeling in design for co-firing biomass in wall-fired burners" *Chem Eng Sci*. Vol. 59(16), pp. 3281-3292, 2004
- [16] R. Scharler., and I. Obernberger, "Numerical modeling of biomass grate furnaces" *Proceedings of the 5th European conference on industrial furnaces and boilers*, Porto, Portugal, April, 2000
- [17] Scharler R., Obernberger I., Längle G., and Heinzle J. (2000) CFD analysis of air staging and flue gas recirculation in biomass grate furnace, In: proceeding of the 1st world conference on biomass for energy and industry, Sevilla, Spain,
- [18] M. Mando, L. Rosendahl, C. Yin, H. Sorensen, "Pulverized straw combustion in low-NO_x multifuel burner: Modeling the transition from coal to straw" *Fuel*, Vol. 89, pp. 3051-3062, 2010
- [19] A. Elfasakhany, L. Tao, B. Espenas, J. Larfeldt, X.S. Bai, "Pulverised wood combustion in a vertical furnace: Experimental and computational analyses" *Applied Energy*, Vol. 112, pp. 454-464, 2013
- [20] A. Arafat Bhuiyan, J. Naser, "Numerical modelling of oxy fuel combustion, the effect of radiative and connective heat transfer and burnout" *Fuel*, Vol. 139, pp. 268-284, 2015
- [21] Stroh Alexander, Falah Alobaid, Jan-Peter Busch, Jochen Strohle, Bernd Epple "3-D numerical simulation for co-firing of torrefied biomass in a pulverized-fired 1 MWth combustion chamber" *Energy*, Vol. 85, pp. 105-116, 2015
- [22] M. Obaidullah, S. Bram, V. K. Verma, J. De Ruyck, "A Review on Particle Emissions from Small Scale Biomass Combustion" *International Journal Of Renewable Energy Research*, Vol.2, No.1, 2012
- [23] Hu Manyin Yin Qi Yu Jinxing Zhang Jing "Numerical Simulation of Bag-type Collector Flow Field in Biomass Energy Power Plant" 2009 Sixth International Conference on Fuzzy Systems and Knowledge Discovery. DOI: 10.1109/FSKD.2009.485
- [24] Hu Manyin, Han Jing, Yu Jinxing, Liu Tongxin "Numerical simulation of combustion of circulation fluidized bed biomass boiler" 2009 International Conference on Computational Intelligence and Software Engineering. DOI: 10.1109/CISE.2009.5364541
- [25] D.G.C. Wickramasinghe1, M. Narayana2, A.D.U.S. Amarasinghe3 "Numerical Simulation of Suspension Biomass Combustor with Two Chambers" 2018 Moratuwa Engineering Research Conference (MERCon) DOI: 10.1109/MERCon.2018.8421947
- [26] T.M. Alkhamis, M.M. Kablan, Olive cake as an energy source and catalyst for oil shale production of energy and its impact on the environment, *Energy Conversion & Management* Vol. 40, pp. 1863-1870, 1999
- [27] Y. H. Khraisha, M. A. Hamdan, H. S. Qalalweh. "Direct Combustion of Olive Cake Using Fluidized Bed Combustor" *Energy Sources*, Vol. 21:4, pp. 319-327, 1999
- [28] V. Murat, T. A. Ayse, "Combustion of olive cake and coal in a bubbling fluidized bed with secondary air injection" *Fuel*, Vol. 86, pp. 1430-1438, 2007
- [29] A. Elorf, N. Mrad, T. Boushaki, B. Sarh, J. Chaoufi, S. Bostyn, I. Gokalp, "Swirl motion effects on flame dynamic of pulverized olive cake in vertical furnace" *Comb. Sci. Technol.* Vol. 188, pp. 1951-1971, 2016
- [30] ANSYS® Academic Research. Release 14.0. Help System. FLUENT User Guide. ANSYS Inc.
- [31] B.E. Launder, and B.D. Spalding, "Lectures in Mathematical models of turbulence" London, UK. Academic Press, 1972
- [32] K. Gautham, R. Rajesh and J. S. Philip, Parallelization of the P-1 Radiation Model, *Numerical Heat Transfer, Part B: Fundamentals*, vol. 49, pp. 1-17, 2006.
- [33] W. P., Jones, J. H. Whitelaw, "Calculation methods for reacting turbulent flows: A review" *Combustion & Flame*, Vol. 48, pp. 1-26, 1982

- [34] J. E. MACPHEE, M. SELIER, M. JERMY and E. TADULAN, "CFD Modelling of pulverized coal combustion in a rotary lime kiln" Seventh International Conference on CFD in the Minerals and Process Industries, CSIRO, Melbourne, Australia, 9-11 December 2009.
- [35] M., Oevermann, S. Gerber, F. Behrendt, "Euler-Lagrange/DEM simulation of wood gasification in a bubbling fluidized bed reactor" Particuology, Vol. 7, pp. 307-316, 2009
- [36] Ravi Inder Sing, Anders Brink, Mikko Hupa "CFD modeling to study fluidized bed combustion and gasification" Applied Thermal Engineering, Vol. 52, pp. 585-614, 2013